Science Bulletin 64 (2019) 1496–1501

Contents lists available at ScienceDirect

Science Bulletin

journal homepage: www.elsevier.com/locate/scib

Science Bulletin
www.scibull.com

Article

De Haas–van Alphen study on three-dimensional topological semimetal pyrite $PtBi_2$

Wenshuai Gao [a,b,c,1], Xiangde Zhu [b,1], Jin Hu [e], Shujing Li [f], Fawei Zheng [f], Hongwei Zhang [b,c], Min Wu [b,c], Guolin Zheng [b,c,g], Ning Hao [b], Ping Zhang [f], Wei Ning [b,*], Mingliang Tian [a,b,d,*]

[a] Institute of Physical Science and Information Technology, School of Physics and Materials Science, Anhui University, Hefei 230601, China
[b] Anhui Province Key Laboratory of Condensed Matter Physics at Extreme Conditions, High Magnetic Field Laboratory, Chinese Academy of Sciences, Hefei 230031, China
[c] Department of Physics, University of Science and Technology of China, Hefei 230026, China
[d] Collaborative Innovation Center of Advanced Microstructures, Nanjing University, Nanjing 210093, China
[e] Department of Physics, Institute for Nanoscience and Engineering, University of Arkansas, Fayetteville, AR 72701, USA
[f] Institute of Applied Physics and Computational Mathematics, Beijing 100088, China
[g] Schoo of Science, RMIT University, Melbourne, VIC3001, Australia

ARTICLE INFO

Article history:
Received 14 May 2019
Received in revised form 9 July 2019
Accepted 19 July 2019
Available online 9 August 2019

Keywords:
Topological semimetal
Pyrite $PtBi_2$
De Haas–van Alphen effect
Fermi surface topology

ABSTRACT

We present the systematic de Haas–van Alphen (dHvA) quantum oscillations studies on the recently discovered topological Dirac semimetal pyrite $PtBi_2$ single crystals. Remarkable dHvA oscillations are emerged at a low field about 1.5 T. From the analyses of the dHvA oscillations, we extract the high quantum mobilities, light effective masses and phase shift factors for the Dirac fermions in pyrite $PtBi_2$. From the angular dependence of the dHvA oscillations, we map out the topology of the Fermi surface. Furthermore, we identify two additional oscillation frequencies that are not probed by the SdH oscillations, which provides us with opportunities to further understand its Fermi surface topology.

1. Introduction

Three-dimensional (3D) topological semimetals, including Dirac and Weyl semimetals, have recently attracted huge interests [1–12]. The relativistic fermions hosted by Dirac and Weyl cones usually exhibit rich exotic transport phenomena such as the negative magnetoresistance (MR) induced by chiral anomaly, extremely large and linear MR. These properties are mostly relative to their non-trivial Berry's phase [13,14], light effective electron mass [13] and ultrahigh mobility [15]. Such characteristics of the relativistic fermions can be identified by measuring the Shubnikov–de Haas (SdH) quantum oscillation due to the field-induced evolution of the Landau levels. The de Haas–van Alphen (dHvA) effect, oscillatory variation of the diamagnetic susceptibility as a function of magnetic field, is another powerful method of probing Fermi surface topology. Compared to the SdH effect that results from the scattering rate of charge carriers, the magnetization oscillations originate from the free energy in presence of the magnetic field, so the dHvA effect is insensitive to the quantum interference effects and provides a more accurate picture of Fermi surface. Recently, the dHvA effect has gained extensive attention in probing the band topology of topological materials, such as the typical Dirac semimetal Cd_3As_2 [16], the nodal-line semimetal ZrSiX (X = S, Se, Te) [17–19] and the Weyl semimetal $TaIrTe_4$ [20].

The recently discovered pyrite $PtBi_2$ has been proposed to be a 3D topological semimetal with extreme large MR [21] and unique electronic structure [21,22]. Except for the flat electron pocket near the Γ-point, an electron pocket near the *R*-point and a hole pocket near the *M*-point were identified by SdH quantum oscillations of the MR measurements. In this work, we report the magnetization study on pyrite $PtBi_2$ single crystals and observe the prominent dHvA quantum oscillations at a low field about $B = 1.5$ T. Signatures of the relativistic fermions in pyrite $PtBi_2$ are observed, including light effective masses and high quantum mobilities. Interestingly, except for the two oscillation frequencies from α and β -bands, we detect two additional frequencies, which provide us with opportunities to further understand its Fermi surface topology.

* Corresponding authors.
E-mail addresses: ningwei@hmfl.ac.cn (W. Ning), tianml@hmfl.ac.cn (M. Tian).
[1] These authors contributed equally to this work.

https://doi.org/10.1016/j.scib.2019.08.005
2095-9273/

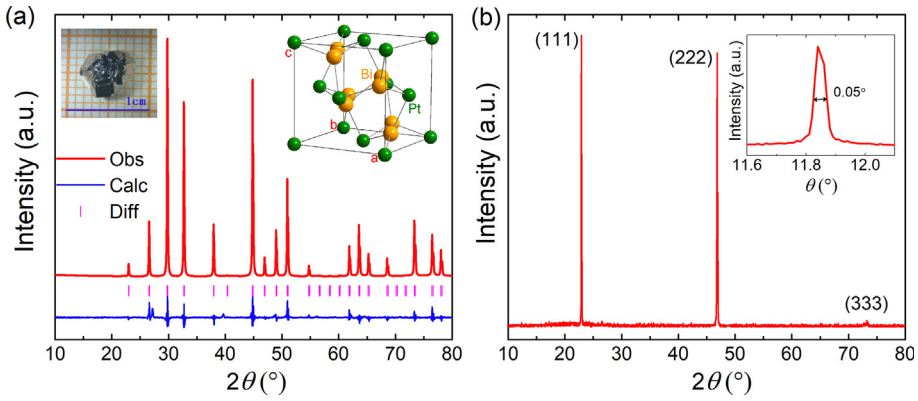

Fig. 1. (Color online) X-ray diffraction (XRD) pattern of pyrite $PtBi_2$. (a) XRD pattern of powdered pyrite $PtBi_2$ at room temperature. Inset: image of a single crystal (left) and crystal structure (right). (b) XRD pattern of (1 1 1) plane of single crystal sample. Inset: the rocking curve of the (1 1 1) diffraction peak, showing the full width at half maximum of 0.05°.

2. Methods

High-quality pyrite $PtBi_2$ single crystals (top left corner of Fig. 1a, inset) were prepared by Bi-flux method. The raw materials with mol ratio Pt:Bi = 1:16 were put in an alumina crucible, then put and sealed it in a quartz tube under vacuum. The tube was heated up to 600 °C and dwelled for 24 h, then slowly cooled to 300 °C with a rate of 2 °C per hour. At this temperature, the flux was separated by a centrifuge. Structural characterization on single-crystal samples was measured with the Rigaku-TTR3 X-ray diffractometer using the high intensity graphite monochromatized Cu Ka radiation. The angular dependent magnetization measurements were carried out on a 7 T superconducting quantum interference device magnetometer (SQUID, Quantum Design, Inc.) by using a standard sample holder with rotation stage. The angular dependence of dHvA oscillation spectra was obtained by subtracting the smooth background of magnetization.

The electronic structure of pyrite $PtBi_2$ was obtained by performing an *ab initio* calculation. We employed the Vienna ab-initio simulation package (VASP) [23–25] for first-principles calculations. The generalized gradient approximation (GGA) of Perdew-Burke-Ernzerhof (PBE) [26] type was used to treat the exchange-correlation potential. Spin-orbit coupling (SOC) was taken into account self-consistently. The crystal structures were fully relaxed until the residual force on each atom was less 0.01 eV $Å^{-1}$. To characterize the Fermi surface, we used the Wannier90 softwave package to consider the maximally localized Wannier function (MWLF) [27,28] for *d* orbitals of Pt and *p* orbitals of Bi.

3. Results and discussions

The excellent crystallinity is demonstrated by the sharp X-ray diffraction (XRD) peaks as shown in Fig. 1b, where the full width at half maximum of the rocking curve reaches as low as 0.05° (Fig. 1b, inset). Through the Rietveld refinement of the power XRD spectrum, the lattice parameters are identified with $a = b = c = 6.704(5)$ Å and $\alpha = \beta = \gamma = 90°$ (top right corner of Fig. 1a, inset), which is consistent with the previous reported results [29]. Fig. 2a shows the magnetization M as a function of the magnetic field B at $T = 2$ K when the field is applied perpendicular to (1 1 1) plane. As we can see, strong magnetization oscillation arises at a low field about $B = 1.5$ T. The oscillatory component M is striking after removing the smooth magnetization background, as shown in the inset of Fig. 2b. The fast Fourier transformation (FFT) spectrum of M reveals two major frequencies, $F_\alpha = 204$ T and $F_\beta = 730$ T. According to the Onsager relation $F = (\hbar/2\pi e)A_F$, the extreme cross sections of Fermi surface are determined to be 0.019(4) and 0.069(5) $Å^{-2}$ for the α and β pockets, respectively. In

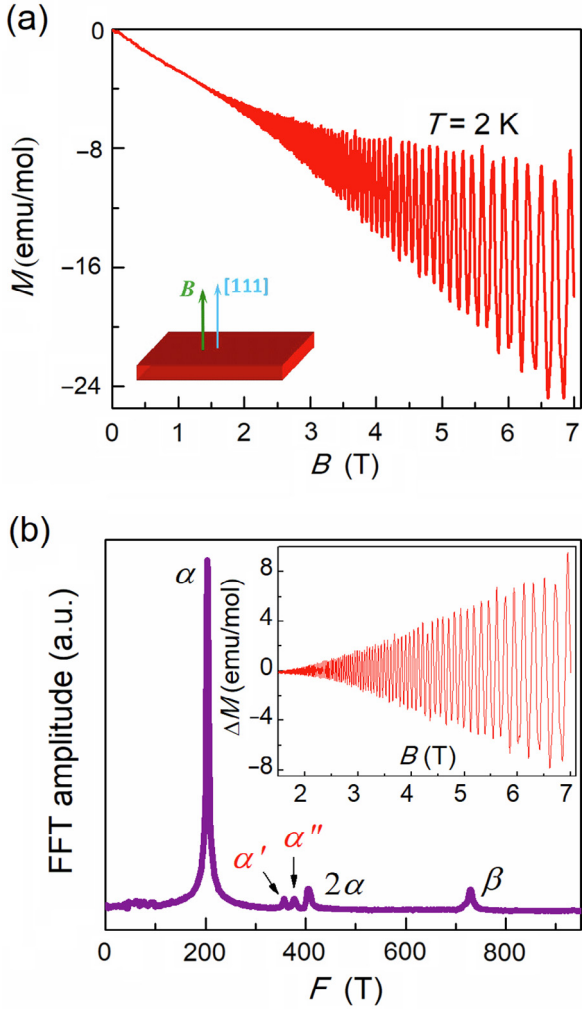

Fig. 2. (Color online) Magnetization oscillation and FFT spectrum at 2 K. (a) Magnetic field dependence of the magnetization at $T = 2$ K with a magnetic field aligned perpendicular to (1 1 1) plane. (b) The corresponding FFT spectrum of the dHvA oscillation. Inset: the oscillatory component of the dHvA effect as a function of *B*.

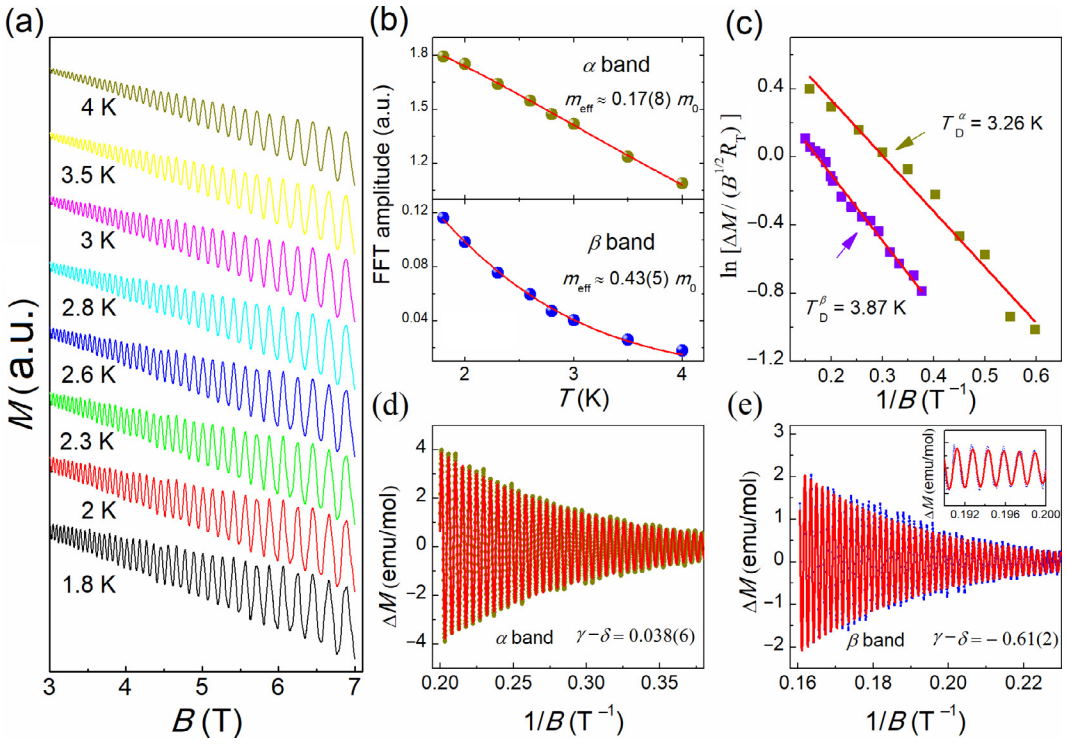

Fig. 3. (Color online) (a) Magnetic field dependence of magnetization at different temperatures when the magnetic field is aligned perpendicular to (1 1 1) plane. Data have been shifted for clarity. (b) Temperature dependence of the corresponding FFT amplitudes, the solid lines represent the fit for effective mass. (c) Dingle plot of the α and β pockets, and the red lines are the fitting result. (d) and (e) Lifshitz-Kosevich (LK) fit (red line) of dHvA oscillation pattern of α pocket (yellow circles) and β pocket (blue circles).

addition to these two major frequencies, we also notice two additional frequencies near the 2nd harmonic frequency of F_α, marked as $F_{\alpha'}$ and $F_{\alpha''}$ in Fig. 2b, which has not been observed in the previous SdH oscillation studies [21]. As will be discussed latter, these additional frequencies result from the hole Fermi pockets near the *M*-point in the first Brillouin zone, which enable us to further investigate the electronic properties of pyrite $PtBi_2$.

The magnetization measurements at various temperatures are performed to obtain the effective mass of the α and β pockets. Given the weak F_β oscillation component damps quickly with rising temperature, the measurements focus on the relative lower temperature range from 1.8 to 4 K, as shown in Fig. 3a. The amplitude of the oscillations decreases gradually with increasing temperatures. The dHvA oscillations are often described using the Lifshitz-Kosevich (LK) formula [30,31]:

$$\Delta M \propto -B^{\frac{1}{2}} R_T R_D \sin\left[2\pi\left(\frac{F}{B}+\gamma-\delta\right)\right], \quad (1)$$

where $R_T = \alpha T/\sinh\alpha T$, $R_D = \exp(-\alpha T_D m^*/B)$, T_D is the Dingle temperature and $\alpha = 2\pi^2 k_B m^*/\hbar eB$. k_B is the Boltzmann constant, $\hbar$ is the Planck's constant, m^* is the effective cyclotron mass at the Fermi energy. Through fitting the temperature dependence of the FFT amplitudes using the thermal damping term of the LK formula, $\frac{2\pi^2 k_B T m^*/\hbar eB}{\sinh\left[2\pi^2 k_B T m^*/\hbar eB\right]}$, we can get the value of m^*. As shown in Fig. 3b, the best fittings yield the effective masses of $m^*_\alpha = 0.17(8)m_0$ and $m^*_\beta = 0.43(5)m_0$ (m_0 is the free electron mass) for the α and β pockets, respectively. Both the effective masses are lighter than the previous results obtained from the SdH oscillations [21], especially for the α pocket where the effective mass is about four times smaller than the transport result. Similar behaviors have been observed in other reported topological semimetals, for examples, the effective mass from the dHvA oscillations measurement in the nodal-line semimetal ZrSiS (or in the Dirac semimetal LaBi) is about 3 (or 2) times smaller than that from the SdH oscillations [32–34]. As we know, the dHvA effect is an equilibrium state behavior, where the oscillatory magnetization is related to the oscillations of the density of states. The SdH effect is a nonequilibrium dynamics effect, except for the density of states, it is also closely related to the electron scattering rate, which has the same oscillation period with the density of states. However, the electron scattering can be complicated by some mechanisms, such as the lattice scattering, the impurity scattering and the inter/inner-Landau level scattering [35]. Take them into account, the amplitude of SdH oscillation is only an approximate expression, which will further affect the value of effective mass.

Besides, by fitting the dHvA oscillation amplitudes with the inverse magnetic field to the Dingle damping termsexp $(-2\pi^2 k_B T_D/\hbar\omega_c)$, we can obtain Dingle temperature of both frequencies. To achieve more accurate fits, we separate the oscillation components of α and β pockets through filtering out the irrelevant oscillations, then we extract the oscillation amplitude of 2 K as a function of $1/B$. As shown in Fig. 3c, the best linear fittings based on the transformational LK formula yield Dingle temperatures $T_D^\alpha = 3.26 \pm 0.26$ K and $T_D^\beta = 3.87 \pm 0.31$ K, respectively. The quantum scattering lifetime τ_Q, which is related to Dingle temperature by $\tau_Q = \hbar/2\pi k_B T_D$, are $\tau_Q^\alpha = 3.7(4) \times 10^{-13}$ s and $\tau_Q^\beta = 3.1(5) \times 10^{-13}$ s. The quantum mobilities estimated by $\mu_Q = \frac{e\tau_Q}{m^*}$, are $\mu_Q^\alpha = 3940.4$ cm^2 V^{-1} s^{-1} and $\mu_Q^\beta = 1299.6$ cm^2 V^{-1} s^{-1}, respectively. Such quantum mobilities are higher than the ones obtained from the SdH oscillations.

In addition to the light effective mass and high mobility, the Berry phase close to π is another important characteristic for the topological non-trivial band. The Landau level (LL) index fan diagram has been widely used to extract the Berry phase for topological materials. However, for the oscillations containing multiple frequencies, the phase factor for each frequency component is bet-

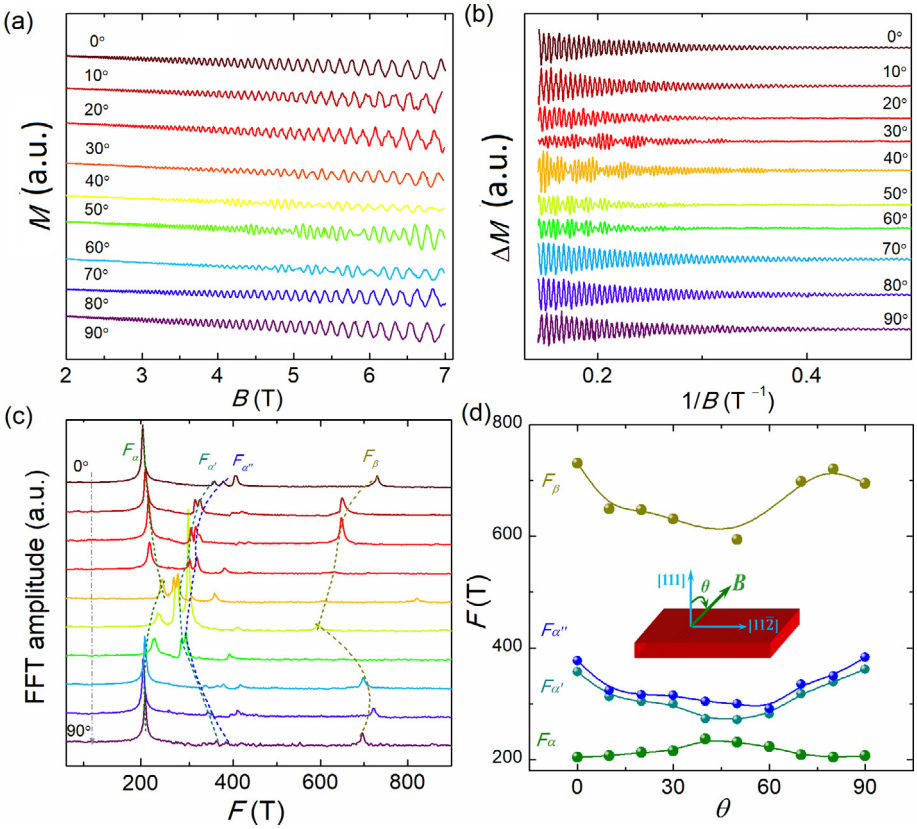

Fig. 4. (Color online) Angular dependences of oscillation frequencies. (a) Magnetic field dependence of magnetization at different angles at $T = 2$ K. Data at different field orientations have been shifted for clarity. (b) The shifted dHvA oscillations as a function of $1/B$ at different angles. (c) The shifted FFT spectra for different angles. (d) The angular dependences of the oscillation frequencies of both α and β pockets. Inset: the schematic configuration for angular dependent measurement of magnetization.

ter to be extracted by fitting the oscillation pattern to the LK formula [14,21]. As shown in the Fig. 3d and e, we separate the oscillation components of α and β pocket through filtrating frequencies. With the effective mass, frequency and Dingle temperature of each band extracted from the dHvA oscillations as the fixed parameters, we expect to duplicate the oscillation pattern through adjusting the phase factor. The LK formula reproduces each oscillation pattern very well and yields a phase factor $\gamma - \delta$ of 0.038 and –0.61 for α and β pocket, respectively. The phase factor of β pocket is very close to –5/8, which indicates a nontrivial Berry phase of the β band [21].

To investigate the Fermi surfaces topology of pyrite $PtBi_2$, we perform the angular-dependence of dHvA effect measurements with the magnetic field rotate from out of plane to in-plane direction, as shown in Fig. 4a. In Fig. 4b we depict the oscillation components with the magnetization background removed. Although the dHvA oscillation patterns vary with the field orientations, the oscillations remain to be strong when rotating the field direction, indicating a 3D Fermi surface for pyrite $PtBi_2$. From the FFT spectra of the oscillation patterns (Fig. 4c), we extract the angular-dependences (0° for [1 1 1] plane and 90° for [1 1 $\bar{2}$] plane) of the oscillation frequencies. As shown in Fig. 4d, with the angle increasing, F_α increasing gradually and then decreasing slowly, the maximum value appears around $\theta = 45°$. However, the $F_{\alpha'}$ and $F_{\alpha''}$ display the opposite evolutionary trend relative to F_α, the minimum of them appear also around $\theta = 45°$ and nearly cross the frequency F_α. For F_β , the evolution with the angle is more complex, indicating a more complicated Fermi surface of the β band.

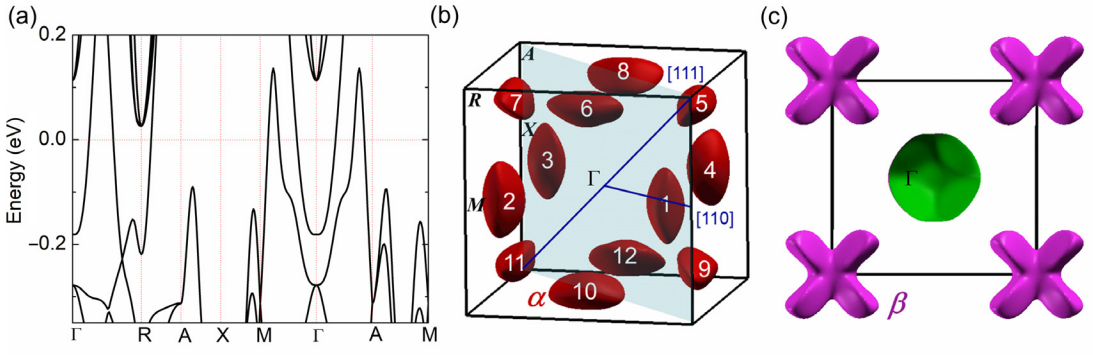

Fig. 5. (Color online) Band structure and Fermi surface. (a) The calculated band structure of pyrite-type $PtBi_2$. (b)The calculated α hole pockets in the first Brillouin zone. (c) The top view of electron pockets in the first Brillouin zone.

Table 1
Several characteristic parameters derived from the dHvA and SdH oscillations of α and β pockets. F, the oscillation frequency; m_{eff}, the effective mass; v_F, the Fermi vector; T_D, the Dingle temperature; μ_Q, the quantum mobility.

Pockets			α					β		
Quantities	F (T)	m_{eff} (m_0)	v_F (10^5 m s^{-1})	T_D (K)	μ_Q (cm^2 V^{-1} s^{-1})	F (T)	m_{eff} (m_0)	v_F (10^5 m s^{-1})	T_D (K)	μ_Q (cm^2 V^{-1} s^{-1})
dHvA	204	0.17(8)	5.3(5)	3.26	3940.4	730	0.43(5)	4.0(1)	3.87	1299.6
SdH	250	0.64(1)	1.58	7.4	453.4	850	0.68(1)	2.76	10.6	298.7

According to the calculated band structure, as shown in Fig. 5a, there are three pockets, including two electron pockets located around the Γ and R point and a hole pocket crossed by the Γ-M line. The β pockets alone Γ- R are Dirac linear dispersion with topological protection. According to the previous SdH effect study [21], the α and β pockets correspond to the hole and electron pockets around the M and R points, respectively. To understand the division of α frequencies in the dHvA effect, we plot the α pockets separately from other pockets in the first Brillouin zone (Fig. 5b and c). As shown in Fig. 5b, the twelve ellipsoid-like hole Fermi surface pockets (labeled by 1–12) are not equivalent with the principal axes pointing different directions. By analyzing the experimental setup (Fig. 4d, inset) and the angular dependences of frequencies, we propose that the hole pockets give rise to the observed oscillation frequencies F_α, $F_{\alpha'}$ and $F_{\alpha''}$. More specifically, for the strong anisotropy of α pockets in pyrite $PtBi_2$, when the magnetic field is parallel to [1 1 0] direction, the inequivalence twelve α pockets are divided into three groups in the first Brillouin zone. Each group contributes a different extremal cross section when the magnetic field is fixed along a specific direction, resulting in three different oscillation frequencies. The $F_{\alpha'}$ and $F_{\alpha''}$ result from the oscillations of Fermi pockets in group 1 (Nos. 1, 3) and 2 (Nos. 2, 4) while the main frequency F_α is from the oscillation of Fermi pockets in group 3 (Nos. 5–12). As change the magnetic direction from [1 1 1] to [1 1 $\bar{2}$], the extremal cross-sections of group 1 and 2 decrease firstly and then increase gradually, resulting in the same evolution of the frequencies $F_{\alpha'}$ and $F_{\alpha''}$. The location of the pockets in group 3 are great different from that of group 1 and 2. When rotate the field direction, the cross-sections increase firstly and then decrease and so does the behavior of F_α. Therefore, compared with the SdH oscillations that only probed the F_α frequency [21], the dHvA effect provides opportunities to investigate the complete hole Fermi surface pockets that is not accessible to the SdH oscillations. As for F_β, i.e. the light electron (pink) Fermi surfaces located around the R point of the first Brillouin zone are equivalent, so we detect only one oscillation frequency.

To make a comparison of the results between the SdH oscillations and dHvA effect, we summarize the major characteristic parameters in Table 1. Both the main dHvA oscillation frequencies are slightly lower than those of the SdH results. The magnetization measurements also reveal the lighter effective carrier masses and higher quantum mobilities than those from the transport results. As we know, the dHvA effect can be well interpreted by the Lifshitz-Kosevich theory. Although the SdH effect is an analogous effect on the electrical resistance and shares the same physics of the quantized Landau level picture with the former, there is still delicate difference between them. Take the scattering of electrons into account, the original Lifshitz-Kosevich theory is more precise to describe the dHvA effect originated from the oscillations of free energy. As a result, the dHvA oscillations will give a lighter effective mass and a smaller Dingle temperature of both pockets, resulting in the high quantum mobilities in pyrite $PtBi_2$. The dHvA oscillations also detect additional frequencies compared with the SdH oscillations, which provide more accurate information of the Fermi surface. Additionally, we note that the effective masses are obtained in the field range of 1.5–7 T for the dHvA oscillations while 18–33 T for the SdH oscillations. The selected different field range between dHvA and SdH oscillations may also affect the effective mass values for Dingle term. As we know, the effective mass is obtained by fitting the LK formula with an average $1/\bar{B}$, the different field range may give an error due to the exponential decay of the envelope function of oscillations. When we get the FFT spectra and analyze the effective masses, we select the inverse field window contained the remarkable dHvA oscillations that within the influence of the Dingle factor.

4. Conclusion

In conclusion, we have performed the dHvA oscillation studies on the Dirac semimetal pyrite $PtBi_2$ using magnetization measurements. Strong dHvA quantum oscillations are observed at a low field about $B = 1.5$ T. The analyses of oscillation patterns reveal high quantum mobilities, light effective masses and nontrivial Berry phase for the Dirac fermions in pyrite $PtBi_2$. Compared to the transport results, the effective masses obtained from the magnetization measurements are smaller and the quantum mobilities are higher. The electron scattering may result in such differences of two methods. The angular dependences of oscillation frequencies help us to understand its anisotropic complex electronic structure more clearly. Furthermore, two additional frequencies $F_{\alpha'}$ and$F_{\alpha''}$are detected besides the two frequencies F_α and F_β, which provide us with opportunities to further investigate the topology of Fermi surface in pyrite $PtBi_2$.

Conflict of interest

The authors declare that they have no conflict of interest.

Acknowledgments

This work was supported by the National Key Research and Development Program of China (2016YFA0401003), the National Natural Science Foundation of China (11774353, 11574320, 11204312, 11674331, 11474289, 11804340, and U1732274), the Youth Innovation Promotion Association of Chinese Academy of Sciences (2017483), the Innovative Program of Development Foundation of Hefei Center for Physical Science and Technology (2018CXFX002), the Chinese Academy of Sciences Pioneer Hundred Talents Program and the Natural Science Foundation of Anhui Province (1908085QA15).

Author contributions

X.D.Z. synthesized the single crystals. W.S.G. and H.W.Z characterized the crystal structure. The magnetization measurements in the 7T SQUID were carried out by W.S.G with the assistance of M.W. and. G.L.Z. F.Z., S.J.L., N.H. and P.Z. performed the ab initio calculations and theoretical analyses. W.S.G., W.N., N.H., J.H. and M.L. T. wrote the paper and conducted data analyses. All authors contributed to scientific discussions and commented on the manuscript.

References

[1] Orlita M, Basko DM, Zholudev MS, et al. Observation of three-dimensional massless kane fermions in a zinc-blende crystal. Nat Phys 2014;10:233–8.
[2] Wan XG, Turner AM, Vishwanath A, et al. Topological semimetal and Fermi-arc surface states in the electronic structure of pyrochlore iridates. Phys Rev B 2011;83:205101.
[3] Wang ZJ, Sun Y, Chen XQ, et al. Dirac semimetal and topological phase transitions in A_3Bi (A=Na, K, Rb). Phys Rev B 2012;85:195320.
[4] Young SM, Zaheer S, Teo JCY, et al. Dirac semimetal in three dimensions. Phys Rev Lett 2012;108:140405.
[5] Fang C, Gilbert MJ, Dai X, et al. Multi-weyl topological semimetals stabilized by point group symmetry. Phys Rev Lett 2012;108:266802.
[6] Xu SY, Liu C, Kushwaha SK, et al. Observation of Fermi arc surface states in a topological metal. Science 2014;347:294–8.
[7] Lv BQ, Muff S, Qian T, et al. Observation of Fermi-arc spin texture in TaAs. Phys Rev Lett 2015;115:217601.
[8] Liu ZK, Jiang J, Zhou B, et al. A stable three-dimensional topological Dirac semimetal Cd_3As_2. Nat Mater 2014;13:677–81.
[9] Borisenko S, Gibson Q, Evtushinsky D, et al. Experimental realization of a three-dimensional Dirac semimetal. Phys Rev Lett 2014;113:027603.
[10] Liu ZK, Zhou B, Zhang Y, et al. Discovery of a three-dimensional topological dirac semimetal, Na_3Bi. Science 2014;343:864–7.
[11] Furusaki A. Weyl points and dirac lines protected by multiple screw rotations. Sci Bull 2017;62:788–94.
[12] Xiong J, Kushwaha SK, Liang T, et al. Evidence for the chiral anomaly in the Dirac semimetal Na_3Bi. Science 2015;350:413–6.
[13] He LP, Hong XC, Dong JK, et al. Quantum transport evidence for the three-dimensional dirac semimetal phase in Cd_3As_2. Phys Rev Lett 2014;113:246402.
[14] Hu J, Liu JY, Graf D, et al. π Berry phase and zeeman splitting of Weyl semimetal TaP. Sci Rep 2016;6:18674.
[15] Liang T, Gibson Q, Ali MN, et al. Ultrahigh mobility and giant magnetoresistance in the Dirac semimetal Cd_3As_2. Nat Mater 2015;14:280–4.
[16] Pariari A, Dutta P, Mandal P. Probing the Fermi surface of three-dimensional Dirac semimetal Cd_3As_2 through the de Haas–van Alphen technique. Phys Rev B 2015;91:155139.
[17] Hu J, Tang ZJ, Liu JY, et al. Nearly massless Dirac fermions and strong Zeeman splitting in the nodal-line semimetal ZrSiS probed by de Haas–van Alphen quantum oscillations. Phys Rev B 2017;96:045127.
[18] Hu J, Tang ZJ, Liu JY, et al. Evidence of topological nodal-line fermions in ZrSiSe and ZrSiTe. Phys Rev Lett 2016;117:016602.
[19] Hu J, Zhu YL, Graf D, et al. Quantum oscillation studies of the topological semimetal candidate ZrGeM (M=S, Se, Te). Phys Rev B 2017;95:205134.
[20] Khim S, Koepernik K, Efremov DV, et al. Magnetotransport and de Haas–van Alphen measurements in the type-II Weyl semimetal $TaIrTe_4$. Phys Rev B 2016;94:165145.
[21] Gao WS, Hao NN, Zheng FW, et al. Extremely large magnetoresistance in a topological semimetal candidate pyrite $PtBi_2$. Phys Rev Lett 2017;118:256601.
[22] Zhao LX, Xu LC, Zuo HK, et al. Fermi surface and carrier compensation of pyrite-type $PtBi_2$ revealed by quantum oscillations. Phys Rev B 2018;98:085137.
[23] Kresse G, Hafner J. Ab initio molecular-dynamics simulation of the liquid-metal–amorphous-semiconductor transition in germanium. Phys Rev B 1994;49:14251.
[24] Kresse G, Furthmüller J. Efficiency of ab-initio total energy calculations for metals and semiconductors using a plane-wave basis set. Comput Mater Sci 1996;6:15.
[25] Kresse G, Furthmüller J. Efficient iterative schemes for ab initio total-energy calculations using a plane-wave basis set. Phys Rev B 1996;54:11169.
[26] Perdew JP, Burke K, Ernzerhof M. Generalized gradient approximation made simple. Phys Rev Lett 1996;77:3865.
[27] Marzari N, Vanderbit D. Maximally localized generalized Wannier functions for composite energy bands. Phys Rev B 1997;56:128427.
[28] Souza I, Marzari N, Vanderbit D. Maximally localized Wannier functions for entangled energy bands. Phys Rev B 2001;65:035109.
[29] Furuseth S, Selte K, Kjekshus A. Redetermined crystal structures of $PdAs_2$, $PdSb_2$, PtP_2, $PtAs_2$, $PtSb_2$, α-$PtBi_2$, and $AuSb_2$. Acta Chem Scand 1965;19:735–41.
[30] Lifshitz IM, Kosevich AM. Theory of magnetic susceptibility in metals at low temperatures. Sov Phys JETP 1956;2:636.
[31] Mikitik GP, Sharlai YV. Manifestation of Berry's phase in metal physics. Phys Rev Lett 1999;82:2147.
[32] Matusiak M, Cooper JR, Kaczorowski D. Thermoelectric quantum oscillations in ZrSiS. Nat Commun 2017;8:15219.
[33] Singha R, Satpati B, Mandal P. Fermi surface topology and signature of surface Dirac nodes in LaBi. Sci Rep 2017;7:6321.
[34] Sun S, Wang Q, Guo P-J, et al. Large magnetoresistance in LaBi: origin of field-induced resistivity upturn and plateau in compensated semimetals. New J Phys 2016;18:082002.
[35] Admas EN, Holstein TD. Quantum theory of transverse galvano-magnetic phenomena. J Phys Chem Sol 1959;10:254.

Wenshuai Gao received his Ph.D. degree from the University of Science and Technology of China (USTC) in 2018. His current research interest focuses on the novel quantum properties of topological materials and low dimensional quantum materials.

Wei Ning received his Ph.D. degree from Institute of Physics, Chinese Academy of Sciences in 2009. He is currently a research scientist in High Magnetic Field Laboratory, Chinese Academy of Sciences. His research interest focuses on the electrical transport investigation of novel low-dimensional topological materials.

Mingliang Tian received his Ph.D. degree from Wuhan University in 1992. He is currently a senior research scientist in the field of experimental condensed matter physics in High Magnetic Field Laboratory, the Chinese Academy of Sciences, Hefei City. His research interest covers the physical phenomena of low dimensional quantum materials (e.g., superconducting, magnetic and topological materials) under extreme condition.